

Geophysical Research Letters

RESEARCH LETTER

10.1029/2018GL081399

Key Points:

- Isentropic stream function shows a robust expansion toward smaller pressure and broadening of MSE in a warming climate
- While upward mass transport decreases in global average, upward MSE transport increases, mostly due to the eddies
- An increase of effective MSE range is found globally, especially in the subtropics

Supporting Information:

- Supporting Information S1

Correspondence to:

Y. Wu,
yutianwu@ldeo.columbia.edu

Citation:

Wu, Y., Lu, J., & Pauluis, O. (2019). Weakening of upward mass but intensification of upward energy transport in a warming climate, *Geophysical Research Letters*, 46. <https://doi.org/10.1029/2018GL081399>

Received 20 NOV 2018

Accepted 21 JAN 2019

Accepted article online 28 JAN 2019

Weakening of Upward Mass but Intensification of Upward Energy Transport in a Warming Climate

Yutian Wu¹ , Jian Lu² , and Olivier Pauluis³

¹Lamont-Doherty Earth Observatory of Columbia University, Palisades, NY, USA, ²Division of Atmospheric Sciences and Global Change, Pacific Northwest National Laboratory, Richland, WA, USA, ³Courant Institute of Mathematical Sciences, New York University, New York, NY, USA

Abstract How the atmospheric overturning circulation is projected to change is important for understanding changes in mass and energy budget. This study analyzes the overturning circulation by sorting the upward mass transport in terms of the moist static energy (MSE) of air parcels in an ensemble of coupled climate models. It is found that, in response to greenhouse gas increases, the upward transport of MSE increases in order to balance the increase in radiative cooling of the mass transport. At the same time, the overall mass transport decreases. The increase in energy transport and decrease in mass transport can be explained by the fact that the MSE of rising air parcels increases more rapidly than that of subsiding air, thus allowing for a weaker overturning circulation to transport more energy.

Plain Language Summary The atmospheric circulation transports energy upward to balance the energy loss due to radiative cooling. This energy transport is the direct result of the fact that rising air parcels are typically warmer and moister than subsiding air and thus have a higher-energy content. It is shown here that as the amount of greenhouse gases increases, the upward energy transport increases while the mass transport weakens. This apparent discrepancy can be explained by the fact that, in a warmer world, the energy content of rising air increases more rapidly than that of subsiding air, making the atmospheric circulation more efficient at transporting energy upward.

1. Introduction

It is well recognized that the atmosphere transports energy from the surface to the free atmosphere in order to balance radiative cooling. This energy transport is achieved through a combination of rising warm, moist air and descending cold, dry air. This overturning occurs through a wide range of atmospheric motions, including convection, midlatitude eddies, and planetary-scale flows such as the Hadley and Walker cells. In this paper, we analyze how an increase in greenhouse gas concentration affects both the atmospheric overturning and the associated energy transport.

Here we quantify the atmospheric overturning by computing a mass transport in pressure and moist static energy (MSE) coordinates. To do so, we sort the vertical mass flux as a function of the MSE of the air parcels. This technique was introduced by Pauluis and Mrowiec (2013) and has been used to study hurricane (Mrowiec et al., 2016), moist convection (Pauluis, 2016), tropical circulation (Slawinska et al., 2016), and the global atmospheric circulation (Laliberte et al., 2015). This isentropic method makes it possible to identify the resolved overturning circulation that is directly associated with the vertical energy transport and to naturally filter out the transport by gravity waves and other reversible oscillatory motions. Moreover, the isentropic framework is advantageous in depicting the heat engine and the closed thermodynamic cycle of the atmosphere. A particular challenge in studying the upward energy transport lies in the broad range of motions that it involves, from convective updrafts on the scale of a few hundreds of meters to the planetary-scale Hadley and Walker cells. One of the benefits of the isentropic analyses to tackle this problem lies in that it does not impose an a priori scale separation but rather includes all resolved scales of motions involved in the overturning.

How the upward transport of mass and MSE changes with anthropogenic climate change is important in understanding the atmospheric energy balance and its change but is not yet entirely clear. Held and Soden (2006) analyzed a number of coupled climate models that participated in the Coupled Model

Intercomparison Project phase 3 (CMIP3) and found, in addition to a robust intensification of the hydrological cycle, a decrease in convective mass flux as a result of anthropogenic CO₂ increase. They argued that the decrease in convective mass flux is a consequence of thermodynamic constraints and is consistent with the larger increase in atmospheric water vapor than the increase in precipitation. They also examined the change in tropical convective mass flux simulated in one model and found the dominance by a decrease in the stationary eddy component and, to a lesser extent, a decrease in the zonal mean component. In the extratropics, the eddies play an important role in transporting both mass and energy upward; however, how they are projected to change has not yet been carefully studied, except the well-established poleward shift of the storm tracks (Yin, 2005). Therefore, we aim to construct the global overturning circulation using the isentropic framework and to investigate the anthropogenic changes in the future warming climate.

Previous studies have used a similar isentropic framework to study the global atmospheric circulation and its future change. For example, Laliberte et al. (2015) investigated the atmospheric entropy budget and work output of the atmospheric heat engine using thermodynamic diagrams in temperature-moist entropy space and in specific humidity-chemical potential space. They found that the work output is always less than that of an equivalent Carnot cycle due to the power needed to maintain the hydrological cycle. They also examined the future warming simulation in one climate model and found that, in the global average, the stream function in temperature-entropy space strengthens at higher moist entropy values while weakening at lower moist entropy values and the stream function in specific humidity-chemical potential space strengthens almost uniformly everywhere. As a result, this implies a decrease in work output in the future warming climate due to the larger increase in the hydrological cycle than the increase in total entropy production. In addition, Laliberte and Pauluis (2010) and Wu and Pauluis (2013) analyzed the atmospheric meridional circulation on latitude-(equivalent) potential temperature space. They found that, in response to a CO₂ increase, while the wintertime midlatitude circulation weakens on potential temperature surfaces, on equivalent potential temperature surfaces, it shows a poleward shift with an intensification on the poleward flank due to the intensified eddy moisture transport in the middle to high latitudes. Kjellsson (2015) calculated the stream function in dry static energy and latent heat space by including the advection of dry static energy from the zonal, meridional, and vertical directions and found a weakening of the global atmospheric circulation in the annual average. The discrepancy between previous studies could be due to the differences in the methodology and the seasons analyzed, but that is not the focus of this study.

In this paper, we aim to complement previous studies and to investigate the resolved vertical branch of the atmospheric circulation, its associated upward transport of mass and energy in an ensemble of climate models, and their response to anthropogenic climate change. This paper is organized as follows. In section 2, we describe the methodology in constructing the isentropic stream function and the CMIP5 data sets. In section 3, we present the anthropogenic climate change response in the isentropic stream function and associated upward transport of mass and energy. Section 4 concludes the paper.

2. Methods and Data

2.1. Methodology

The methodology here is analogous to studies of the atmospheric meridional circulation in isentropic coordinates (e.g., Held & Schneider, 1999; Pauluis et al., 2008, 2010). We calculate the stream function for the vertical velocity of the global atmospheric circulation in MSE (M_0) and pressure (p) space

$$\Psi(M_0, p) = \frac{1}{\tau} \int_0^\tau \int_{-\pi/2}^{\pi/2} \int_0^{2\pi} H[M_0 - M]H[p_s - p] \frac{1}{g} \omega a^2 d\lambda d\phi dt, \quad (1)$$

where $M = C_p T + gZ + L_v q$ is the MSE with T temperature, Z geopotential height, q specific humidity, $C_p = 1,004$ J/K, $g = 9.8$ m/s², and $L_v = 2.5 \times 10^6$ J/kg. The τ is the time period over which the averaging is performed, λ denotes longitude, ϕ is the latitude, p_s is surface pressure, ω is pressure velocity, and $a = 6.37 \times 10^6$ m is the Earth's radius. H is Heaviside function with $H(x) = 1$ if $x \geq 0$ and $H(x) = 0$ otherwise. The stream function defined here corresponds to the net upward mass transport by all air parcels with MSE smaller than the threshold M_0 .

Furthermore, this stream function can be decomposed into zonal mean Ψ_{zm} and eddy component Ψ_{eddy} :

$$\Psi = \Psi_{zm} + \Psi_{eddy}, \quad (2)$$

$$\Psi_{\text{zm}}(M_0, p) = \frac{1}{\tau} \int_0^\tau \int_{-\pi/2}^{\pi/2} \int_0^{2\pi} H[M_0 - M]H[p_s - p] \frac{1}{g} \langle \omega \rangle a^2 d\lambda d\phi dt, \quad (3)$$

$$\Psi_{\text{eddy}}(M_0, p) = \frac{1}{\tau} \int_0^\tau \int_{-\pi/2}^{\pi/2} \int_0^{2\pi} H[M_0 - M]H[p_s - p] \frac{1}{g} \omega^* a^2 d\lambda d\phi dt, \quad (4)$$

where $\langle \omega \rangle = \frac{\int_0^{2\pi} \omega H(p_s - p) d\lambda}{\int_0^{2\pi} H(p_s - p) d\lambda}$ is zonally averaged vertical velocity and $\omega^* = \omega - \langle \omega \rangle$ is the deviation from the zonal mean component. The eddy component of the stream function thus includes both the stationary and transient eddies.

Based on the isentropic stream function, the associated net upward transport of mass can be calculated as follows:

$$m(p) = \max_{M_0} \Psi - \min_{M_0} \Psi. \quad (5)$$

The transport of MSE can be calculated as follows:

$$F(p) = \int_{M_0, \text{min}}^{M_0, \text{max}} M_0 \frac{\partial \Psi}{\partial M_0} dM_0 = - \int_{M_0, \text{min}}^{M_0, \text{max}} \Psi dM_0, \quad (6)$$

with M_0, min and M_0, max denoting the minimum and maximum of MSE, respectively. The second equality is due to the stream function decaying to zero when the MSE value is sufficiently small or large. Additionally, we define the effective MSE range as the ratio of the upward MSE transport and the upward mass transport

$$M_{\text{eff}} = \frac{F}{m}, \quad (7)$$

and it measures the MSE difference between the saturated ascent and the environmental descent and thus the efficiency associated with the upward transport.

Moreover, the eddy stream function can be further decomposed by latitude by defining a local eddy stream function

$$\psi_{\text{eddy}}(M_0, \phi, p) = \frac{1}{\tau} \int_0^\tau \int_0^{2\pi} H[M_0 - M]H[p_s - p] \frac{1}{g} \omega^* a^2 d\lambda dt. \quad (8)$$

This local eddy stream function vanishes at both high and low values of MSE, and one can apply equations (5)–(7) to defined an eddy mass transport, eddy energy transport, and eddy effective range as a function of latitude and pressure.

2.2. CMIP5 Output

We use the daily output of temperature, geopotential height, specific humidity, and pressure velocity and monthly output of surface pressure from 14 CMIP5 models (their run 1) with available model output. The isentropic stream function is calculated for both the historical scenario during 1981–2000 and the Representative Concentration Pathway (RCP) 8.5 scenario during 2081–2100. All the results to be shown are annual averages.

3. Results

3.1. Simulated Climatology and Response in Globally Averaged Isentropic Stream Function

We begin by discussing the results in globally averaged isentropic stream function. Figure 1 shows both the climatology and future response of the total stream function (calculated following equation (1)) and contributions from the zonal mean and eddy components (calculated following equations (3) and (4)) in CMIP5 multimodel mean. The historical total stream function in multimodel mean, shown in Figure 1a, is similar to that calculated from the European Centre for Medium-Range Weather Forecast ERA-Interim reanalysis data set (not shown; X. Chen, personal communication, October 2018) and shows a single, closed, counterclockwise overturning circulation. As a comparison, the maximum of the overturning stream function calculated using the 6-hourly 0.75° horizontal resolution ERA-Interim reanalysis is about 5×10^{11} kg/s (not shown), while the CMIP5 multimodel mean using daily output is about 4.5×10^{11} kg/s. The overturning circulation is composed of nearly moist adiabatic ascent in the deep tropics with large value of MSE (about

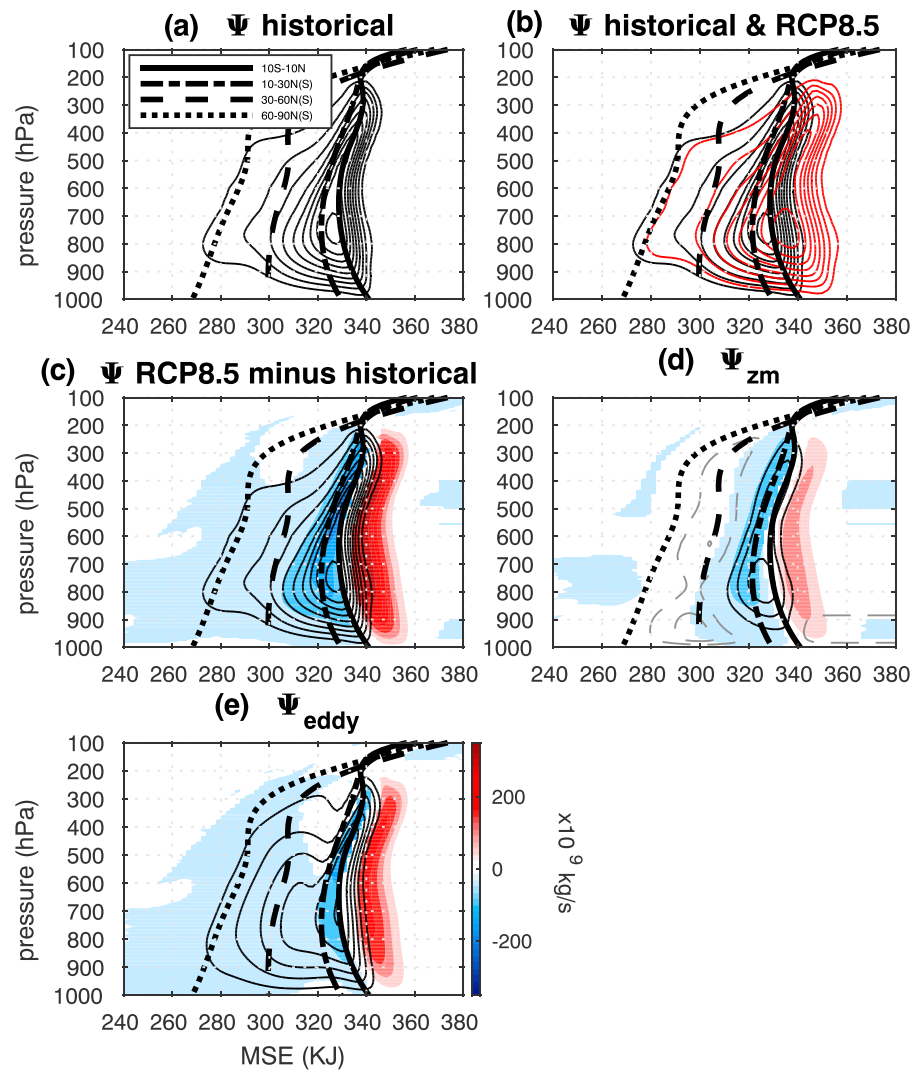


Figure 1. (a) Total isentropic stream function in historical scenario (black contours) and (b) total isentropic stream function in historical scenario (black contours) and RCP8.5 scenario (red contours). Difference in RCP8.5 and historical scenarios in (c) total, (d) zonal mean, and (e) eddy isentropic stream function, shown in color shadings with color bar in (e). The responses are shown when at least 11 out of 14 models agree on the sign of the change. The contours in (c)–(e) plot the historical stream function with black solid contours for positive values while gray dashed for negative values. The contour interval (CI) = 50×10^9 kg/s for (a)–(e) except in (d) -25×10^9 -kg/s contour line is also plotted in order to show the Ferrel cell. The historical MSE values averaged over 10°S to 10°N , 10° to 30°N(S) , 30° to 60°N(S) , and 60° to 90°N(S) are plotted in thick black solid, dash-dotted, dashed, and dotted lines, respectively, as indicated in the legend shown in (a). The stream functions are all shown in global annual mean in multimodel mean. RCP8.5 = Representative Concentration Pathway (RCP) 8.5.

340–350 KJ), descent in all other latitudes accompanied by MSE decrease, and near-surface return flow with MSE increase.

Furthermore, the total stream function can be decomposed into the zonal mean component and the eddy component. The climatological zonal mean component consists of a Hadley circulation in the tropics and a much weaker Ferrel cell in the midlatitudes with a reversed overturning (see contours in Figure 1d). The eddy component shows two branches, that is, a tropical branch representing the Walker cell with a deep vertical extent and concentrated, large MSE values, and a midlatitude branch covering a wide range of MSE (see contours in Figure 1e). The compensation between the midlatitude eddies and the Ferrel cell can be seen in Figure 1de with MSE of about 280–320 kJ.

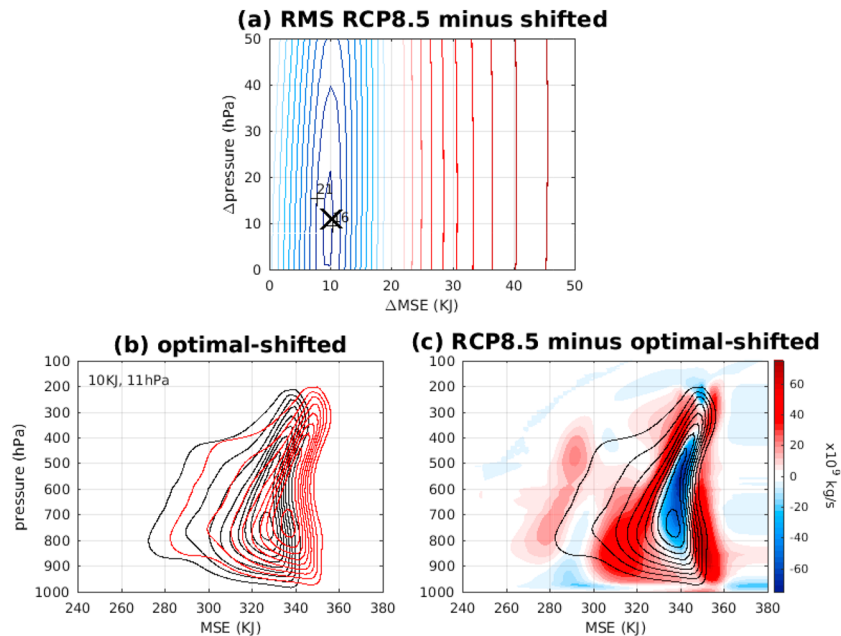


Figure 2. (a) Square root of the mean square (RMS) difference between the RCP8.5 stream function and the shifted historical stream function averaged over all pressure and MSE grid points as a function of MSE increase and pressure decrease. The CI = 5×10^9 kg/s and black cross indicates the minimum of the RMS difference. (b) The historical stream function (black contours) and the optimal shifted historical stream function (red contours) with CI = 50×10^9 kg/s. The optimal shifted stream function corresponds to the black cross in (a) where the minimum of RMS difference is found with a 10-KJ increase in MSE and a 11-hPa upward shift (also indicated in the upper left corner of the plot). (c) Difference between the RCP8.5 stream function and the optimal shifted historical stream function (color shadings, note the different color bars as compared to Figure 1). Black contours plot the optimal shifted historical stream function with CI = 50×10^9 kg/s. RCP8.5 = Representative Concentration Pathway 8.5; MSE = moist static energy.

Figure S1 in the supporting information shows the climatological total stream function in individual models. While models all exhibit a similar overturning circulation, differences can be found among models. As found in cloud-resolving model simulations in Pauluis and Mrowiec (2013), the isentropic mass transport is maximized near the Earth’s surface, corresponding to a strong overturning associated with shallow convection. However, while the CMIP5 multimodel mean shows a stream function that is maximized in the lower troposphere (Figure 1a), some models show a maximum in the upper and middle troposphere. This deficiency might be a result of the parameterized convection in models—for models whose parameterized shallow convection is too strong or deep convection is too weak, the compensating large-scale circulation is likely shifted to the upper and middle troposphere, resulting in a stream function maximum there.

In response to anthropogenic greenhouse gas increase (Figure 1b), the RCP8.5 total stream function, compared to the historical stream function, shows a broadening of the overturning in MSE, especially in the ascent region, and an upward expansion toward smaller pressure. This results in an increase of the stream function in the deep tropics and a decrease in all other latitudes including where the historical stream function maximum is located (Figure 1c). This expansion toward larger MSE was also found in one climate model analysis in Laliberte et al. (2015) (see their Figure 3a) and is a robust feature in CMIP5 models (Figure S1). This shift is also seen in both the zonal mean and eddy components (Figures 1d, 1e, S2, and S3), with a larger response in the eddy component.

3.2. Upward Expansion and MSE Broadening

Next we explicitly quantify the amount of MSE increase and vertical shift for the global annual mean overturning. More specifically, we determine the shifts in pressure and MSE by minimizing the square root of the mean square (RMS) difference between the RCP8.5 total stream function and the shifted historical total stream function averaged over all pressure and MSE grid points. In the multimodel mean, we find a minimum in RMS difference and a corresponding optimal shift of about 10-KJ MSE increase and 11-hPa upward shift (Figure 2a). Figure 2b shows both the historical stream function and the optimal shifted stream function. The results in individual models are shown in Figure S4 with MSE increase of 8–14 KJ and upward shift

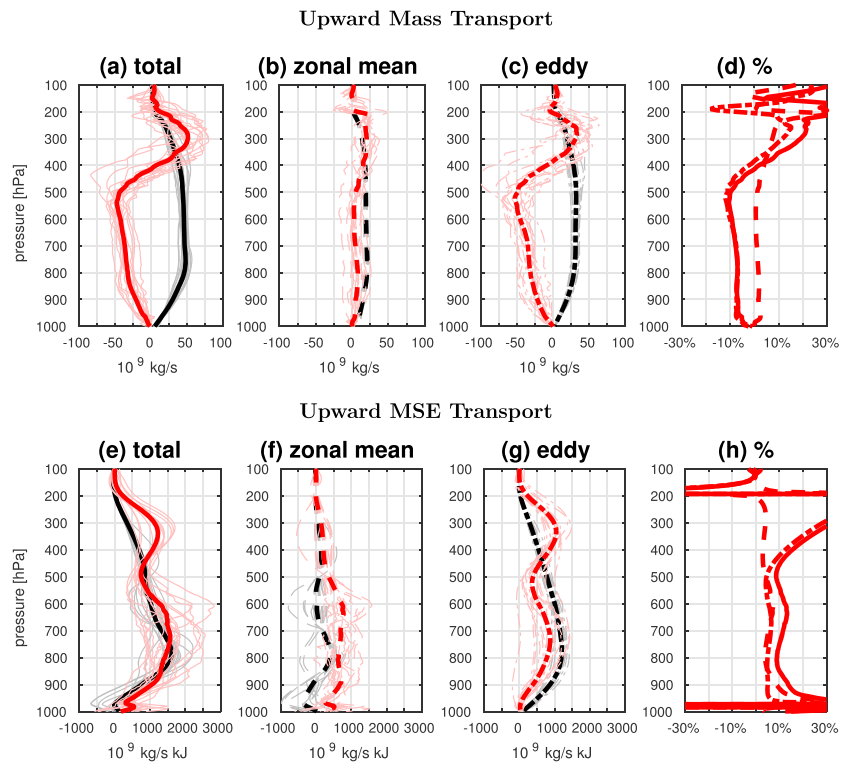


Figure 3. The upward transport of mass in global average accomplished by (a) total, (b) zonal mean, and (c) eddy isentropic stream function, calculated following equation (5). The climatology from the historical scenario is scaled by a factor of 0.1 and is shown in black and the anthropogenic response (i.e., difference between the RCP8.5 and historical scenario) is shown in red. The results from individual models are plotted in thin lines and those from the multimodel mean are plotted in thick lines. (d) The percentage change (i.e., response divided by total historical climatology) for total (solid), zonal mean (dashed), and eddy (dash dotted) components, respectively, in multimodel mean. (e)–(h) Similar to (a)–(d) except for the upward transport of MSE, calculated following equation (6).

of 5–15 hPa among the CMIP5 models analyzed here. Figure 2c shows the difference between the RCP8.5 and the optimal shifted historical stream function and is the residual after removing the effect due to global mean MSE increase and upward lift. Figure S5 shows the results in individual models, and they all look alike. First, the residual is found to be much smaller than the response shown in Figure 1c (note the different color bars), which suggests the dominance of the effect of MSE increase and upward lift. Second, the residual in the ascending branch still shows a shift toward larger MSE, due to the larger MSE increase in the tropics than in the global mean. The residual in the descending branch shows an increase of the stream function, which is in contrast to the decrease of the stream function as shown in Figure 1c. This increase of the stream function is particularly located in the subtropical region of descent and likely corresponds to an expansion of the stream function toward higher latitudes (e.g., Davis et al., 2017; Lu et al., 2007) and thus smaller MSE.

Here we explain the increase in global annual mean MSE using thermodynamic scaling. First, we estimate MSE using its near-surface value: $MSE \approx C_p T_{srf} + L_v q_{srf}$. Then the change in MSE due to anthropogenic greenhouse gas increase and surface temperature increase can be approximated as $\Delta MSE \approx \frac{\Delta T_{srf}}{T_{srf}} (C_p T_{srf} + L_v q_{srf} \frac{L_v}{RT_{srf}})$ by making use of the Clausius-Clapeyron relationship. Therefore, for $T_{srf} = 288$ K and $\Delta T_{srf} = 3.5$ K in multimodel mean under the RCP8.5 scenario, $\frac{\Delta MSE}{MSE} \approx 3.64\%$ and $\Delta MSE \approx 11.3$ KJ, which is consistent with what is found in the optimal shift approach as in Figure 2. Figure S6 shows the scatter plot of global annual mean surface temperature increase versus the optimal shift in MSE among the CMIP5 models, and they are found to be well correlated (correlation is 0.76 and is statistically significant at the 95% level).

For the upward shift of the global mean isentropic stream function, we find a multimodel mean shift of 11 hPa. An upward shift in the tropopause height (e.g., Lorenz & DeWeaver, 2007; Lu et al., 2007) and atmospheric circulation such as the storm tracks (e.g., Singh & O’Gorman, 2012; Yin, 2005) has been

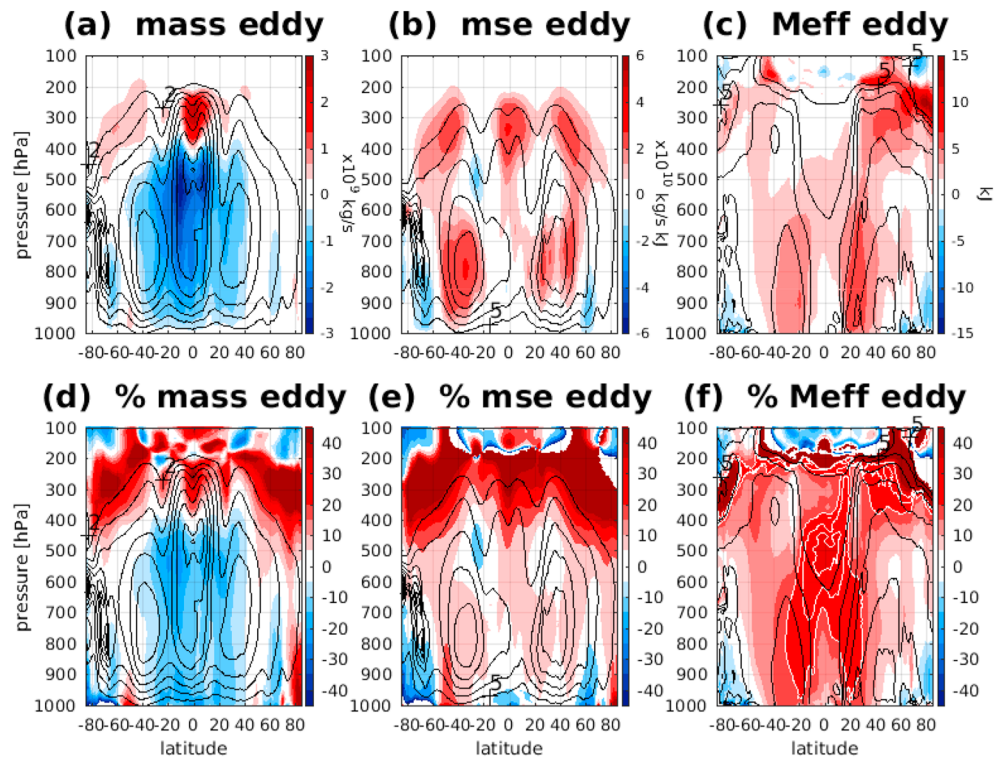


Figure 4. Response in upward transport of (a) mass and (b) MSE by the eddies and (c) the effective MSE range by the eddies (color shadings). The black contours show the climatology from the historical scenario with (a) $CI = 2 \times 10^9$ kg/s, (b) $CI = 5 \times 10^{10}$ kg/s kJ, and (c) $CI = 5$ kJ. (d–f) Similar to (a–c) except that the color shadings show the percentage changes (i.e., response divided by historical climatology). The white contours in (f) highlight the 20%, 25%, and 30% increase of effective MSE range. MSE = moist static energy.

consistently found in anthropogenic climate change simulations. Lu et al. (2007) related the poleward expansion of the Hadley cell to the rise of the extratropical tropopause and found the two positively correlated in anthropogenic climate change response. They also documented that the tropical tropopause rises by about 3.5 hPa/K, and the extratropical tropopause rises by 5 hPa/K in multimodel mean (see their Figure 3). This corresponds to about 4 hPa/K in the global average and, for a 3.5 K temperature increase, a 14-hPa rise in tropopause height, which is similar to the amount of the upward lift of the isentropic stream function found above.

3.3. Response in Upward Mass and MSE Transport

Now we proceed to the analysis of the upward mass and MSE transport simulated by the CMIP5 models. Figures 3a–3d show the climatology and response in globally averaged net upward mass transport that is calculated following equation (5). In climatology, in multimodel mean, the total mass transport is maximized in the lower troposphere (46.3×10^{10} kg/s at 800 hPa, as an example, shown in Figure 3a) and is largely attributed to the eddy component (28.7×10^{10} kg/s at 800 hPa, shown in Figure 3b) and, to a lesser extent, the zonal mean component (20.4×10^{10} kg/s at 800 hPa, shown in Figure 3c). Note that the mass transport is not linearly additive due to the maximum function. In response to anthropogenic climate change, with a global mean surface temperature increase of 3.5 K (Figure S6), the upward total mass transport in global mean multimodel mean decreases by about 7.0% at 800 hPa, and an increase in mass transport can be seen in the upper troposphere, likely due to the rise of the tropopause (see Figures 3a and 3d). This decrease in total mass is dominated by the decrease in the eddy component (see Figures 3c and 3d; about 6.9% decrease at 800 hPa), while the zonal mean component shows a small increase in multimodel mean (see Figures 3b and 3d; about 1.7% increase at 800 hPa).

For the net upward transport of MSE (calculated following equation (6)), the globally averaged climatology is also maximized in the lower troposphere, primarily due to the contribution from the eddies, as shown in Figures 3e–3g. For example, at 800 hPa, the total upward MSE transport in global mean multimodel mean is

about 1.6×10^{13} kg/s kJ, of which 0.4×10^{13} kg/s kJ is due to the zonal mean circulation and 1.2×10^{13} kg/s kJ is due to the eddies. However, in contrast to the weakening of the upward mass transport, the total upward MSE transport shows an increase in the entire troposphere column, especially in the upper troposphere, due to the rise of the tropopause. The increase is due to the contribution from both the eddies and the zonal mean circulation. For example, at 800 hPa, the total MSE transport increases by 9.0% with the zonal mean and eddy components contributing to 4.0% and 4.9%, respectively, as shown in Figure 3h.

Furthermore, for the eddy component, since the eddy stream function is closed at every latitude, we also examine the dependence of the transport of mass and MSE and associated effective MSE range on latitude (shown in Figure 4). While the climatological upward mass transport is maximized in the tropics, the MSE transport is maximized in the midlatitudes, which results in large effective MSE range in the subtropics. Under the RCP8.5 scenario, the upward mass transport decreases in the troposphere with the largest decrease in the tropics (10–20% reduction as shown in Figure 4d) and also shifts upward in the upper troposphere (see Figure 4a). In contrast, the upward transport of MSE intensifies in the troposphere, mainly in the upper troposphere, likely due to the rise in tropopause height, and midlatitude lower troposphere (5–10% increase as shown in Figure 4e; see Figure 4b). As a result, this leads to a significant increase in the effective MSE range, especially in the subtropical middle to lower troposphere and tropical middle troposphere by about 20–30% (see Figures 4c–4f).

Since effective MSE range measures the difference in MSE between the saturated ascent and the environmental descent, it is dominated by the latent energy difference between the saturated ascent and the dry environment and thus can be simply scaled as $M_{\text{eff}} \sim L_v(1 - \text{RH})q^*$, where it is assumed that the ascending motion and the environment have about the same temperature and saturation humidity q^* and RH is the relative humidity of the environment. For the anthropogenic change in M_{eff} , $\Delta M_{\text{eff}} \sim L_v(1 - \text{RH})\Delta q^*$ with ΔRH neglected (e.g., Held & Soden, 2006). This explains why both the climatology and anthropogenic change in M_{eff} are maximized in the subtropics, where RH is small. Indeed, the effective MSE range is found to increase by about 20–30% in the subtropics (shown Figure 4f) and this is mainly because the change in effective MSE range approximately scales with that in saturation humidity, which in turn follows the Clausius-Clapeyron relationship.

4. Conclusion and Discussions

In this study, we have analyzed the thermodynamic processes associated with the atmospheric general circulation in coupled climate models and their response to anthropogenic climate change. More specifically, we have applied isentropic analysis to vertical motion and have constructed the stream function on MSE-latitude-pressure space. We have found that, under the RCP8.5 scenario,

1. The response in globally averaged stream function is primarily characterized by an upward expansion and a broadening in MSE space, the latter satisfying a straightforward thermodynamic scaling resulting from the increase in temperature and humidity. Once the shift toward smaller pressure and larger MSE is accounted for, we observe the additional changes in the overturning circulation: there is a shift toward larger MSE in the deep tropics as the MSE in the tropical region increases more rapidly than the global mean and a weakening of the overturning mass transport.
2. In a global mean sense, the multimodel mean net upward mass transport decreases by about 7% in middle to lower troposphere, mainly due to the eddy component, while the net upward MSE transport increases by about 9%, as a result of the eddies and the zonal mean circulation.
3. Most of the changes in the overturning circulations are tied to changes in the eddy transport, while the contribution from Eulerian mean circulation remains mostly unchanged. The eddy mass transport decreases in the tropics, while the eddy MSE transport increases in the midlatitudes. This implies a weakening of the tropical circulation, partially compensated for by an intensification of the upward energy transport by the synoptic eddies in the midlatitudes.

We stress here that the calculated overturning circulation in this study only takes into account the resolved processes by the models and could be strongly affected by the treatment of convection. Although the isentropic stream function in models is overall similar to that in the ERA-Interim reanalysis, discrepancies are found in model simulations. For instance, there are substantial variations in both the magnitude and location of the maximum of the stream function, both between models, and between models and reanalysis data. Some of these discrepancies are likely related to difference in model resolution and in their treatment of

convection. It is found that the global overturning circulation in the latest ERA5 (30-km spatial resolution) is about 15% stronger than in the ERA-Interim (80-km spatial resolution), with the difference arising primarily from enhanced overturning at the mesoscale (X. Chen, personal communication). It is thus expected that models with a higher spatial resolution should be able to resolve more of the scales responsible for the overturning and thus exhibit a stronger circulation.

Our analysis indicates that, under an anthropogenic increase in greenhouse gases, the CMIP5 models exhibit a systematic reduction in the atmospheric overturning, primarily in the tropical regions, combined with an increase in the upward energy transport, mostly in the midlatitudes. This behavior is robust and found among all CMIP5 models, which reinforces our confidence that it is tied to the fundamental physical mechanisms. Pauluis (2016) also showed that a greenhouse warming leads to a reduction of the atmospheric overturning in a cloud-resolving simulation of radiative-convective equilibrium. The increase in upward MSE transport in CMIP5 is anticipated due to the energetic constraint to balance the increase in radiative cooling due to anthropogenic greenhouse gas increase (e.g., Knutson & Manabe, 1995). For the effective MSE range associated with the net upward transport, its change is dominated by the change of saturation specific humidity in the saturated ascents following the Clausius-Clapeyron relationship and thus increases at a faster rate than that of the radiative cooling. Therefore, as a consequence, this implies a decrease of the net upward mass transport in the future warming climate.

The atmospheric overturning involves a wide range of spatial and temporal scales and as such remains difficult to assess. Over the recent years, tremendous progress has been made toward a better understanding of this key feature of the Earth's climate through a combination of new high-resolution modeling studies, better observational data sets, and new theoretical framework. Yet more work needs to be done, specially to determine the contribution of the smaller scales of motions and to anticipate how the overturning may evolve in a warming climate.

Acknowledgments

The authors thank Dr. Pengfei Zhang for his help in downloading the daily CMIP5 model output. The authors acknowledge the World Climate Research Programme's Working Group on Coupled Modelling, which is responsible for CMIP, and we thank the climate modeling groups for producing and making available their model output. For CMIP the U.S. Department of Energy's Program for Climate Model Diagnosis and Intercomparison provides coordinating support and led development of software infrastructure in partnership with the Global Organization for Earth System Science Portals. The CMIP5 data used in this study are freely available through the Earth System Grid Federation (<https://esgf-node.llnl.gov>).

References

- Davis, N., Birner, T., & Journal of Climate (2017). On the discrepancies in tropical belt expansion between reanalyses and climate models and among tropical belt width metrics, *30*, 1211–1231. <https://doi.org/10.1175/JCLI-D-16-0371.1>
- Held, I. M., & Schneider, T. (1999). The surface branch of the zonally averaged mass transport circulation in the troposphere. *Journal of the Atmospheric Sciences*, *56*, 1688–1697. [https://doi.org/10.1175/1520-0469\(1999\)056<1688:TSBOTZ>2.0.CO;2](https://doi.org/10.1175/1520-0469(1999)056<1688:TSBOTZ>2.0.CO;2)
- Held, I. M., & Soden, B. J. (2006). Robust responses of the hydrological cycle to global warming. *Journal of Climate*, *19*, 5686–5699. <https://doi.org/10.1175/JCLI3990.1>
- Kjellsson, J. (2015). Weakening of the global atmospheric circulation with global warming. *Climate Dynamics*, *45*, 975–988. <https://doi.org/10.1007/s00382-014-2337-8>
- Knutson, T. R., & Manabe, S. (1995). Time-mean response over the tropical pacific to increased CO₂ in a coupled ocean-atmosphere model. *Journal of Climate*, *8*, 2181–2199. [https://doi.org/10.1175/1520-0442\(1995\)008<2181:TMROTT>2.0.CO;2](https://doi.org/10.1175/1520-0442(1995)008<2181:TMROTT>2.0.CO;2)
- Laliberte, F., & Pauluis, O. (2010). Winter intensification of the moist branch of the circulation in simulations of 21st century climate. *Geophysical Research Letters*, *37*, L20707. <https://doi.org/10.1029/2010GL045007>
- Laliberte, F., Zika, J., Mudryk, L., Kushner, P. J., Kjellsson, J., & Doos, K. (2015). Constrained work output of the moist atmospheric heat engine in a changing climate. *Science*, *347*, 540–543. <https://doi.org/10.1126/science.1257103>
- Lorenz, D. J., & DeWeaver, E. T. (2007). Tropopause height and zonal wind response to global warming in the IPCC scenario integrations. *Journal of Geophysical Research*, *112*, D10119. <https://doi.org/10.1029/2006JD008087>
- Lu, J., Vecchi, G. A., & Reichler, T. (2007). Expansion of the Hadley cell under global warming. *Geophysical Research Letters*, *34*, L06805. <https://doi.org/10.1029/2006GL028443>
- Mrowiec, A. A., Pauluis, O. M., & Zhang, F. (2016). Isentropic analysis of a simulated hurricane. *Journal of the Atmospheric Sciences*, *73*, 1857–1870. <https://doi.org/10.1175/JAS-D-15-0063.1>
- Pauluis, O. (2016). The mean air flow as Lagrangian dynamics approximation and its application to moist convection. *Journal of the Atmospheric Sciences*, *73*, 4407–4425. <https://doi.org/10.1175/JAS-D-15-0284.1>
- Pauluis, O., Czaja, A., & Korty, R. (2008). The global atmospheric circulation on moist isentropes. *Science*, *321*, 1075–1078. <https://doi.org/10.1126/science.1159649>
- Pauluis, O., Czaja, A., & Korty, R. (2010). The global atmospheric circulation in moist isentropic coordinates. *Journal of Climate*, *23*, 3077–3093. <https://doi.org/10.1175/2009JCLI2789.1>
- Pauluis, O., & Mrowiec, A. (2013). Isentropic analysis of convective motions. *Journal of the Atmospheric Sciences*, *70*(11), 3673–3688.
- Singh, M. S., & O'Gorman, P. A. (2012). Upward shift of the atmospheric general circulation under global warming: Theory and simulations. *Journal of Climate*, *25*, 8259–8276. <https://doi.org/10.1175/JCLI-D-11-00699.1>
- Slawinska, J., Pauluis, O., Majda, A. J., & Grabowski, W. W. (2016). Multiscale interactions in an idealized walker cell: Analysis with isentropic stream functions. *Journal of the Atmospheric Sciences*, *73*, 1187–1203. <https://doi.org/10.1175/JAS-D-15-0070.1>
- Wu, Y., & Pauluis, O. (2013). Examination of isentropic circulation response to a doubling of carbon dioxide using statistical transformed Eulerian mean. *Journal of the Atmospheric Sciences*, *70*, 1649–1667. <https://doi.org/10.1175/JAS-D-12-0235.1>
- Yin, J. (2005). A consistent poleward shift of the storm tracks in simulations of 21st century climate. *Geophysical Research Letters*, *32*, L18701. <https://doi.org/10.1029/2005GL023684>